



Contents lists available at ScienceDirect

## Ocean Engineering

journal homepage: [www.elsevier.com/locate/oceaneng](http://www.elsevier.com/locate/oceaneng)

## MPS-FEM coupled method for sloshing flows in an elastic tank

Youlin Zhang, Decheng Wan\*

*Collaborative Innovation Center for Advanced Ship and Deep-Sea Exploration, State Key Laboratory of Ocean Engineering, School of Naval Architecture, Ocean and Civil Engineering, Shanghai Jiao Tong University, Shanghai 200240, China*

## ARTICLE INFO

## Keywords:

Moving particle semi-implicit (MPS) method  
Finite element method (FEM)  
Fluid structure interaction (FSI)  
Sloshing  
Roll motion  
MLParticle-SJTU solver

## ABSTRACT

As more and more liquid carriers with huge size are manufactured to support the transportation demand of natural resources, risks such as local deformation or even damage of cargo containment systems resulting from sloshing phenomenon subsequently increase, and it's necessary to take the elasticity of tank walls into account in the researches of sloshing phenomenon. In present paper, we numerically studied the interaction between liquid sloshing flow and elastic bulkheads of liquid carrier by fully Lagrangian particle method, MLParticle-SJTU solver, which is an in-house solver developed based on the moving particle semi-implicit (MPS) method. Coupled with the finite element method (FEM), the MLParticle-SJTU solver is extended to numerical analysis of elastic structural response due to the impact loads of sloshing flows. To validate the feasibility of the MPS-FEM coupled solver in dealing with fluid structure interaction (FSI) problems, a benchmark of dam-breaking flow interacting with elastic lateral wall is studied firstly and results show good agreement with published data. Then, the sloshing phenomenon in an elastic tank is numerically investigated. By varying the Young's modulus of tank walls, interesting characteristics regarding evolutions of free surface, variation of impact pressures, dynamic responses of the structures in both time and frequency domains are presented.

## 1. Introduction

Sloshing in partially filled tanks is a phenomenon that can be observed frequently during liquid bulk cargo carriers operating on rough sea. The high non-linear behavior of sloshing involving violent fluid motion and high impact pressure could potentially cause large deformation on the walls of tanks, loss control of stability or maneuverability of the ship, particularly when the excitation associated with the motion of ship is close to the natural sloshing frequency. The phenomenon, hence, is of great importance in assessing structural strength for designers of liquid cargo carriers.

In the past several decades, this well-known phenomenon has been carefully studied and published in many literatures. Contributions are mainly focused on the evaluation of the extreme impact pressure, the coupling mechanism between ship motions and internal sloshing flows (Zhao et al., 2014; Mitra et al., 2012), techniques to minimize the sloshing (Liu and Lin, 2009) in rigid tanks with model scale. Actually, the tank is usually elastic, particularly for the engineering applications with full scale or the tests with large scale. For instance, the large size bulkheads of the membrane-type tanks are typically elastic structures in liquefied natural gas (LNG) carriers. The deformations of tank walls and

ceilings induced by the impact loads should not be negligible since they are strictly associated with the state of free surface, the level and duration of impact pressure, and finally affect the safety assessment of structure. In view of this, it's necessary to take the influence of the structural responses into account in the researches of sloshing phenomenon.

Until now, several numerical approaches, including the simplified approaches and the fully coupled approaches, have been developed for this fluid structure interaction problem. Two of the typically simplified approaches are so called the spatial simplified approach and the temporal simplified approach for the FSI analysis. For the spatial simplified approach, the 3-D simulations of sloshing in a rigid tank will be conducted firstly, and an overview of the sloshing phenomenon, such as the impact positions and preliminary values of pressure, can be obtained. Then, the 2-D slice which covers the impact location is selected for the FSI analysis with refined grids. This approach has been successfully applied for the assessment of structural safety of cargo containment system (CCS) against sloshing impact loads by Ito et al. (2008). In the work of Lee et al. (2015), a similar treatment called global-local analysis approach is proposed to evaluate the sloshing resistance performance of a huge-size LNG carrier's insulation system. For the temporal simplified approaches, the long duration sloshing impact pressure is usually

\* Corresponding author.

E-mail address: [dcwan@sjtu.edu.cn](mailto:dcwan@sjtu.edu.cn) (D. Wan).

<https://doi.org/10.1016/j.oceaneng.2017.12.008>

Received 28 February 2017; Received in revised form 8 October 2017; Accepted 6 December 2017

Available online xxx

0029-8018/© 2017 Elsevier Ltd. All rights reserved.

idealized by mathematical equations. For instance, Graczyk et al. (2007) and Wang and Kim (2007) simplified the sloshing-induced pressures by triangular or trapezoidal function, and then the idealized loads were applied in the calculation of structural response of the Mark III containment system for LNG. Kim (2015) decomposed the long duration sloshing impact signal into the slowly varied and the rapidly varied component by using the wavelet transform technique. The structural dynamic response was calculated by FEM software under the rapidly varied component of impact load signal approximated by convoluting the wavelet response function and wavelet transform coefficient. Though it is economical for this FSI problem, reliability of the simplified approach is subject to be verified since accuracy of the FSI analysis is strictly linked to the selections of impact locations and the expressions of impact loads.

In comparison with the simplified approaches, accurate pressure time history can be calculated and miscalculation of the impact location could also be avoided based on the fully coupled approaches. Hence, the fully coupled approaches are supposed to be more realistic to the practical phenomenon and thus draw much more attentions of researchers. For example, Idelsohn et al. (2008) applied the particle finite element method (PFEM) for the simulation of the interaction between an elastic structure and free surface flows in a sloshing tank. Fossa et al. (2012) investigated the possible effects of a deformable structure on the sloshing phenomenon with the help of ADINA software which is based on the finite element method (FEM) for both fluid and structural analysis. Liao and Hu (2013) developed a coupling finite difference method (FDM) and the finite element method (FEM) for simulating the interaction between liquid sloshing flow in a rolling tank and a thin elastic plate. Paik and Carrica (2014) developed a coupling nonlinear finite element (FEM) solver and URANS/DES overset solver. The FSI problems of rolling tanks partially filled with fluid interacting with an elastic bar clamped to bottom or top are numerically simulated. Jia et al. (2015) employed the fully coupled approach based on the software ANSYS for solving floating LNG tank sloshing problem in fluid domain for fluid pressure and velocity, and in structure domain for dynamic stresses, dynamic deformation and dynamic reaction forces. Until now, it can be noticed that relatively more numerical researches are carried out by grid-based methods. However, applications of these grid-based methods are restricted by the challenges, e.g. inefficient process of grids generation for complex shape of structure, requirement of dynamic mesh technologies for moving boundary or large structural deformation, simulation of free surface with large deformation or breaking, etc. In view of these points, the Lagrangian meshless methods which are a new generation computational methods for the analysis of fluid physics, are in good performance for these challenges.

In nearly few years, kinds of meshless methods are proposed for free surface flow. One representative meshless particle method is the Moving Particle Semi-Implicit (MPS) method which is originally proposed by Koshizuka and Oka (1996) for incompressible flow. By integrating with the FEM, the MPS method exhibits good performance in FSI problem according to the numerical benchmark test of dam break flow interacting with flexible structure (Mitsume et al., 2014; Sun et al., 2015). However, the application of the MPS-FEM coupled method for the interaction between violent sloshing flow and elastic tank is rarely reported.

In present paper, we aim to develop a MPS-FEM coupled method for the FSI problem of liquid sloshing in a partially filled elastic tank. A fully Lagrangian FSI solver is implemented by extending our in-house MPS solver MLPparticle-SJTU with FEM method for structure analysis. Theories of MPS and FEM method together with the coupling strategy would be presented firstly. Then, the performance of fluid model for violent sloshing flow is verified by the comparison between present numerical result and corresponding experimental data. As a verification of the capability of the MPS-FEM coupled solver for FSI problem, the numerical benchmark of dam break flow impacting onto an elastic lateral wall is simulated and compared with previous published simulation results. Then, the tentative application of present solver for the simulation of sloshing in the elastic tank is conducted. Influence of the structural

elasticity on the impact pressures, deformations of structure and evolutions of free surface of sloshing flow are qualitatively analyzed.

## 2. Numerical methods

In present study, the MPS-FEM coupled method is proposed to address the FSI problems. Herein, formulas of MPS method for fluid domain analysis and FEM for structural domain analysis are briefly introduced. Then, the coupling strategy between fluid solver and structural solver together with the treatments of data transformation on the fluid-structure interface is present.

### 2.1. Fluid solver based on MPS method

#### 2.1.1. Governing equations

Governing equations for incompressible viscous fluid in Lagrangian system are

$$\nabla \cdot \mathbf{V} = 0 \quad (1)$$

$$\frac{D\mathbf{V}}{Dt} = -\frac{1}{\rho}\nabla P + \nu\nabla^2\mathbf{V} + \mathbf{g} \quad (2)$$

where  $\mathbf{V}$ ,  $t$ ,  $\rho$ ,  $P$ ,  $\nu$  and  $\mathbf{g}$  represent the velocity vector, time, water density, pressure, kinematic viscosity and the gravity acceleration vector, respectively.

#### 2.1.2. Kernel function

In particle method, governing equations should be expressed by the particle interaction models based on the kernel function. Here, the kernel function presented by Zhang et al. (2014) is employed.

$$W(r) = \begin{cases} \frac{r_e}{0.85r + 0.15r_e} - 1 & 0 \leq r < r_e \\ 0 & r_e \leq r \end{cases} \quad (3)$$

where  $r$  is distance between particles and  $r_e$  is the effect radius.

#### 2.1.3. Discrete expressions of particle interaction models

The particle interaction models, including the differential operators of gradient, divergence and Laplacian, are defined as

$$\langle \nabla \phi \rangle_i = \frac{dim}{n^0} \sum_{j \neq i} \frac{\phi_j + \phi_i}{|\mathbf{r}_j - \mathbf{r}_i|^2} (\mathbf{r}_j - \mathbf{r}_i) \cdot W(|\mathbf{r}_j - \mathbf{r}_i|) \quad (4)$$

$$\langle \nabla \cdot \Phi \rangle_i = \frac{dim}{n^0} \sum_{j \neq i} \frac{(\Phi_j - \Phi_i) \cdot (\mathbf{r}_j - \mathbf{r}_i)}{|\mathbf{r}_j - \mathbf{r}_i|^2} W(|\mathbf{r}_j - \mathbf{r}_i|) \quad (5)$$

$$\langle \nabla^2 \phi \rangle_i = \frac{2dim}{n^0 \lambda} \sum_{j \neq i} (\phi_j - \phi_i) \cdot W(|\mathbf{r}_j - \mathbf{r}_i|) \quad (6)$$

where  $\phi$  is an arbitrary scalar function,  $\Phi$  is an arbitrary vector,  $dim$  is the number of space dimensions,  $n^0$  is the initial particle number density for incompressible flow,  $\lambda$  is a parameter defined as

$$\lambda = \frac{\sum_{j \neq i} W(|\mathbf{r}_j - \mathbf{r}_i|) \cdot |\mathbf{r}_j - \mathbf{r}_i|^2}{\sum_{j \neq i} W(|\mathbf{r}_j - \mathbf{r}_i|)} \quad (7)$$

which is introduced to keep the variance increase equal to that of the analytical solution  $\lambda = \int_{\mathbf{v}} W(\mathbf{r}) \cdot \mathbf{r}^2 dV / \int_{\mathbf{v}} W(\mathbf{r}) dV$  (Koshizuka et al., 1998).

#### 2.1.4. Model of incompressibility

The incompressible condition of MPS method is represented by keeping the particle number density constant. In each time step, there are

two stages: first, temporal velocity of particles is calculated based on viscous and gravitational forces, and particles are moved according to the temporal velocity; second, pressure is implicitly calculated by solving a Poisson equation, and the velocity and position of particles are updated according to the obtained pressure. The Pressure Poisson Equation (PPE) in present MPS solver is defined as

$$\langle \nabla^2 P^{n+1} \rangle_i = (1 - \gamma) \frac{\rho}{\Delta t} \nabla \cdot \mathbf{V}_i^* - \gamma \frac{\rho}{\Delta t^2} \frac{\langle n^* \rangle_i - n^0}{n^0} \quad (8)$$

where  $\gamma$  is a blending parameter with a value between 0 and 1. The range of  $0.01 \leq \gamma \leq 0.05$  is better according to numerical experiments conducted by Lee et al. (2011). In this paper,  $\gamma = 0.01$  is adopted for all simulations.

### 2.1.5. Free surface particle detection method

For the MPS method, pressure of the fluid domain is closely affected by the accuracy of free surface detection. In present solver, we employ a free surface detection method by Zhang et al. (2014) and defined as

$$\langle \mathbf{F} \rangle_i = \frac{dim}{n^0} \sum_{j \neq i} \frac{1}{|\mathbf{r}_i - \mathbf{r}_j|} (\mathbf{r}_i - \mathbf{r}_j) W(\mathbf{r}_{ij}) \quad (9)$$

where the vector function  $\mathbf{F}$  represents the asymmetry of arrangements of neighbor particles. Particle satisfying

$$\langle |\mathbf{F}| \rangle_i > 0.9 |\mathbf{F}|^0 \quad (10)$$

is considered as free surface particle, where  $|\mathbf{F}|^0$  is the initial value of  $|\mathbf{F}|$  for surface particle.

### 2.2. Structure solver based on FEM

In present paper, extension of the solver MLParticle-SJTU is conducted based on the implicit FEM method for the analysis of structural physics.

According to the FEM theory, the spatially discretized structural dynamic equation, which governs the motion of structural elements, can be expressed as

$$\mathbf{M} \ddot{\mathbf{y}} + \mathbf{C} \dot{\mathbf{y}} + \mathbf{K} \mathbf{y} = \mathbf{F}(t) \quad (11)$$

$$\mathbf{C} = \alpha_1 \mathbf{M} + \alpha_2 \mathbf{K} \quad (12)$$

where  $\mathbf{M}$ ,  $\mathbf{C}$ ,  $\mathbf{K}$  are the structural mass matrix, the Rayleigh damping matrix, the stiffness matrix, respectively. Vector  $\mathbf{F}$  is the external force acting on structure, and varies with computational time. Vector  $\mathbf{y}$  represents the nodal displacement of structure. Coefficients  $\alpha_1$  and  $\alpha_2$  correspond to natural frequencies and damping ratios of structure.

To solve the structural dynamic equation, another two groups of functions should be supplemented to form the equation system closely. Here, Taylor's expansions of velocity and displacement developed by Newmark (1959) are employed:

$$\dot{\mathbf{y}}_{t+\Delta t} = \dot{\mathbf{y}}_t + (1 - \gamma) \ddot{\mathbf{y}}_t \Delta t + \gamma \ddot{\mathbf{y}}_{t+\Delta t} \Delta t, \quad 0 < \gamma < 1 \quad (13)$$

$$\mathbf{y}_{t+\Delta t} = \mathbf{y}_t + \dot{\mathbf{y}}_t \Delta t + \frac{1 - 2\beta}{2} \ddot{\mathbf{y}}_t \Delta t^2 + \beta \ddot{\mathbf{y}}_{t+\Delta t} \Delta t^2, \quad 0 < \beta < 1 \quad (14)$$

where  $\beta$  and  $\gamma$  are selected as  $\beta = 0.25$ ,  $\gamma = 0.5$  for all simulations in present paper. From Eq. (11)–(14), the displacement of structure at  $t = t + \Delta t$  can be solved by the following formula implicitly (Hsiao et al., 1999):

$$\bar{\mathbf{K}} \mathbf{y}_{t+\Delta t} = \bar{\mathbf{F}}_{t+\Delta t} \quad (15)$$

$$\bar{\mathbf{K}} = \mathbf{K} + a_0 \mathbf{M} + a_1 \mathbf{C} \quad (16)$$

$$\bar{\mathbf{F}}_{t+\Delta t} = \mathbf{F}_t + \mathbf{M}(a_0 \mathbf{y}_t + a_2 \dot{\mathbf{y}}_t + a_3 \ddot{\mathbf{y}}_t) + \mathbf{C}(a_1 \mathbf{y}_t + a_4 \dot{\mathbf{y}}_t + a_5 \ddot{\mathbf{y}}_t) \quad (17)$$

$$a_0 = \frac{1}{\beta \Delta t^2}, a_1 = \frac{\gamma}{\beta \Delta t}, a_2 = \frac{1}{\beta \Delta t}, a_3 = \frac{1}{2\beta} - 1, a_4 = \frac{\gamma}{\beta} - 1, \quad (18)$$

$$a_5 = \frac{\Delta t}{2} \left( \frac{\gamma}{\beta} - 2 \right), a_6 = \Delta t(1 - \gamma), a_7 = \gamma \Delta t$$

where  $\bar{\mathbf{K}}$  and  $\bar{\mathbf{F}}$  are so-called effective stiffness matrix and effective force vector, respectively. Finally, the accelerations and velocities corresponding to the next time step are updated as follows.

$$\ddot{\mathbf{y}}_{t+\Delta t} = a_0 (\mathbf{y}_{t+\Delta t} - \mathbf{y}_t) - a_2 \dot{\mathbf{y}}_t - a_3 \ddot{\mathbf{y}}_t \quad (19)$$

$$\dot{\mathbf{y}}_{t+\Delta t} = \dot{\mathbf{y}}_t + a_6 \ddot{\mathbf{y}}_t + a_7 \ddot{\mathbf{y}}_{t+\Delta t} \quad (20)$$

### 2.3. Coupling strategy for FSI problems

In present study, the partitioned coupling strategy between MPS and the FEM method is implemented in the FSI solver since it can take the advantages of code modularity and flexible to enhance the computational accuracy and efficiency. For the development of a partitioned-based FSI solver, the appropriateness and preciseness of its fluid–structure coupling system is one of the crucial issues (Hwang et al., 2014).

Concepts of present coupling system is shown as Fig. 1. The main distinguishing feature of this strategy corresponds to the different sizes of time steps of fluid and structure analysis. According to the Courant–Friedrichs–Lewy (CFL) condition, the fluid time step size  $\Delta t_f$  is commonly set as a much small value. Correspondingly, a much larger structural time step size  $\Delta t_s$  can be utilized in present strategy to improve the calculation efficiency since the Newmark- $\beta$  method, which is employed for structure analysis, is an implicit approach. Here,  $\Delta t_s$  is  $k$  multiples of  $\Delta t_f$ , where  $k$  is an integer. In each cycle of FSI simulation, the fluid analysis is performed based on the MPS solver from the time step  $t_{n+1}$  to  $t_{n+k}$  firstly. Mean pressures of particles on the fluid–structure interface are calculated as

$$\bar{p}_{n+k} = \frac{1}{k} \sum_{i=1}^k p_{n+i} \quad (21)$$

where  $p_{n+i}$  is pressure of the fluid particle on wall boundary at the instant  $t_n + i\Delta t_f$ . For the structure analysis, external force is calculated based on the average pressure  $\bar{p}_{n+1}$  acting on the structure surface and the FEM solver is applied at the time step  $t_{n+k}$ . After structure analysis, position and velocity of structure particles are updated and considered as new boundary conditions for the calculation of fluid physical variables at next time step. Remarkably, position of particles should be updated within the time steps  $t_{n+1}$  and  $t_{n+k-1}$  based on velocity of particles calculated at the

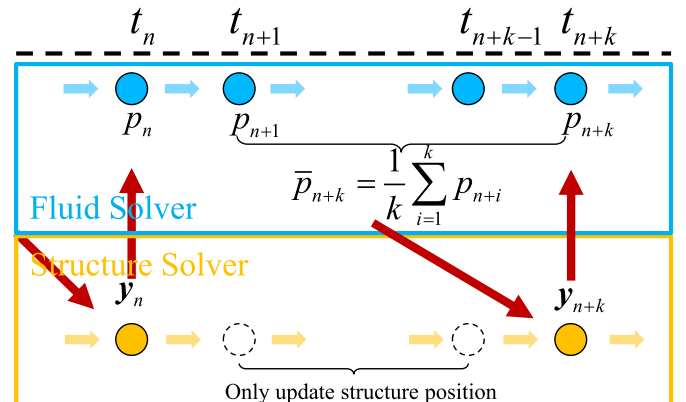


Fig. 1. Concepts of the coupling strategy.

time step  $t_n$  to avoid the instability of fluid field produced by the large displacements of structure particles within  $\Delta t_s$ .

2.4. Data transformation on the fluid-structure interface

In present paper, two-dimension FSI problems are considered and the tank walls will be dispersed to beam elements for the analysis of structural physics. As a result, special treatments need to be implied for data transformation on the fluid-structure interface, including the application of external force onto the beam nodes and the deformation of structural particle model corresponding to the displacements of beam elements. Here, a particle group scheme (Hwang et al., 2016) is considered. Structural particles located within the same section are grouped. For the force transformation, concepts of the numerical considerations are shown as Fig. 2. Herein, the vector  $F_{Gi,l}$  and  $F_{Gi,r}$  represent the force acting on left and right boundary particle of the structural group  $i$ , respectively. As mentioned previously, the pressure of boundary particle is calculated by MPS method initially. Then, force acting on the structural boundary particle within the structural group is calculated by the integration of average pressure acting on the interface. After this, the resultant of forces of particles within the same group are applied onto structural FEM node as the external load for the structural physics analysis. For the deformation of structural particle model, particles within a group move as one body based on the nodal linear velocities  $u_i$

and  $v_i$  which represent the velocities of beam nodes. Then, the final position of structure particles can be updated according to the rotation of group around the center of the section based on the angular velocity  $\omega_i$ . Concepts of the numerical considerations for the deformation of structural particle model are shown as Fig. 3.

3. Validation test of the MPS-FEM coupled solver

As mentioned previously, the bulkheads of partially filled tank may experience nonlinear impact pressures while the liquid container operating on waves. In our previously published works, capability of the MPS solver MParticle-SJTU for violent free surface flows (Tang and Wan, 2015; Tang et al., 2016a, b; Zhang et al., 2016, Zhang and Wan, 2017), including the sloshing flow in a rigid tank (Zhang et al., 2014), has been studied. Herein, feasibility of present solver for FSI problems should be primarily validated before numerically investigating the deformations of tank walls due to the impact loads of sloshing flow. In present section, a numerical benchmark is carried out. The violent dam-breaking flow impacting onto an elastic wall, which shares the features with sloshing flow acting onto elastic tank, is simulated based on the MPS-FEM coupled method.

The benchmark is proposed by Sun et al. (2015) and sketch of the test is shown as Fig. 4. An elastic wall is mounted at right of the tank and corresponding numerical parameters for both structure and fluid analysis

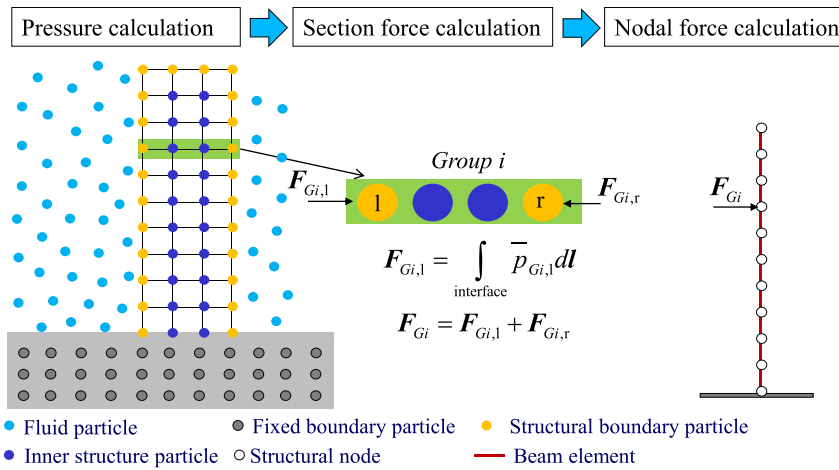


Fig. 2. Concepts of the numerical considerations for force.

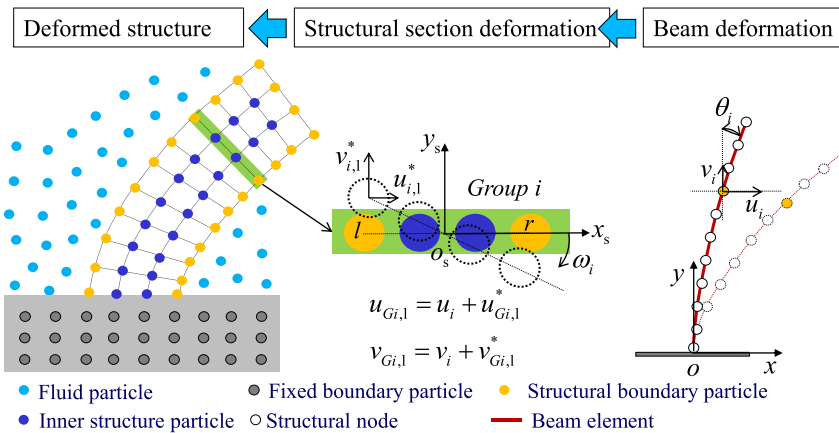


Fig. 3. Concepts of the numerical considerations for deformation of structural particle model.

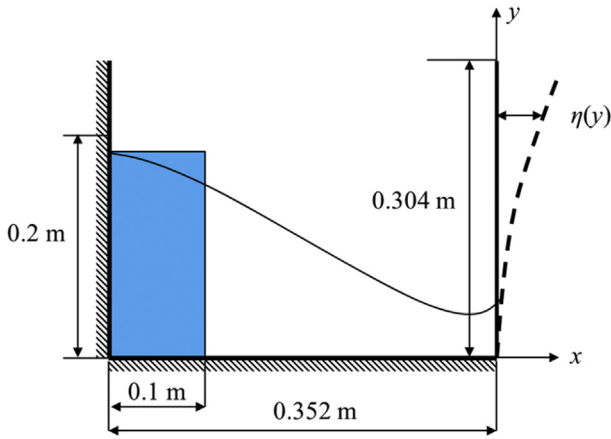


Fig. 4. Schematic Sketch of the dam-breaking with elastic wall.

Table 1  
Parameters of numerical test.

Structure parameters	Values	Fluid parameters	Values
Thickness (m)	0.006	Fluid density (kg/m <sup>3</sup> )	1000
Line density (kg/m)	47.16	Kinematic viscosity (m <sup>2</sup> /s)	1 × 10 <sup>-6</sup>
Young's modulus (GPa)	0.2	Gravitational acceleration (s/m <sup>2</sup> )	9.81
Moment of inertia (m <sup>3</sup> )	1.8 × 10 <sup>-8</sup>	Particle spacing (m)	0.004
Damping coefficients α <sub>1</sub>	0	Total number of particle	1985
Damping coefficients α <sub>2</sub>	0.025	Number of fluid particle	1250
Number of elements	76	Time step size (s)	5 × 10 <sup>-4</sup>
Time step size (s)	0.025		

are presented in Table 1.

Fig. 5 shows the deflection at the top end of the elastic wall versus calculation time. Due to the impact pressure of dam-break water, the wall begins to deform in the positive direction of  $x$  at  $t \approx 0.24$  s, and comes to the maximum at  $t \approx 0.65$  s. Then, the deflection rebounds back with large displacement until  $t \approx 0.9705$  s. Additionally, approximately harmonic vibration of the elastic wall can be observed after  $t \approx 3.0$  s, and presents a frequency closed to the first order of natural angular frequency of the wall ( $\omega = 10.5235$ ). Both trend and amplitude of the deflection curve calculated by present MPS-FEM coupled method agree very well with results published by Sun et al. (2015).

Fig. 6 shows the comparisons of pressure contours, free surface profiles and deformation of beam at four typical time instants. Smooth pressure field can be obtained by present solver, both profiles of free surface and deformation of beam are quite similar with the referred results. So, our coupled MPS-FEM method is dependable for FSI problems with violent free surface.

#### 4. Simulation of sloshing flow in elastic tank

As is well known, the sloshing phenomenon in a rigid tank has been a topic of intensive study for more than four decades, some prominent works about this problem have been carried out. For instance, Faltinsen and Timokha (2009) introduced kinds of approaches for this nonlinear problem systematically, involving the experimental researches, the theoretical and numerical methods. However, precious few literatures focus on the interaction between the sloshing flow and elastic tank walls which is a non-negligible factor in the practical application. By taking the elasticity of tank wall into consideration, various characteristics corresponding to the structural response may be exhibited. In present paper, we focus on the coupling effects resulting from the lateral impact loads in a liquid tank with low

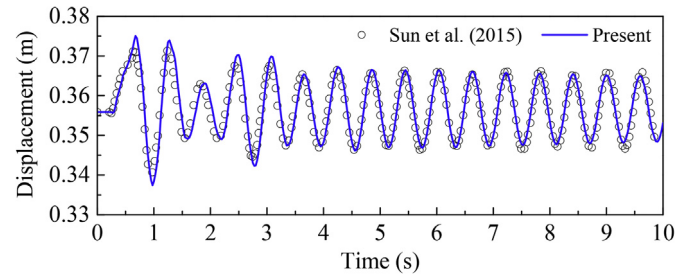


Fig. 5. Comparison study about vibration at the top point of the elastic wall.

filling ratio. Evolutions of free surface, variation of impact pressures, dynamic properties of the structure will be investigated in both time and frequency domain.

#### 4.1. Numerical conditions

According to the experimental results by Souto-Iglesias et al. (2015), violent sloshing flow with impact loads could be observed in a liquid tank with low filling ratio. To investigate the structural response corresponding to the impact loads, the similar numerical conditions are conducted in present paper. Schematic sketch of the tank is shown in Fig. 7, Length ( $L$ ) and height ( $H$ ) of the rectangular tank model are 0.9 m, 0.508 m, respectively. The tank is partially filled with water with the depth  $h = 0.093$  m. Corresponding natural period ( $T_N$ ) of the tank is 1.9191 s, calculated according to the following formula

$$T_N = \frac{2\pi}{\sqrt{\frac{\pi g}{L} \tanh\left(\frac{\pi h}{L}\right)}} \quad (22)$$

A pressure sensor (point S1) is fixed on the lateral tank wall at the reference depth ( $h$ ) while the displacement register (point S2) is at the center of the wall. The rectangular tank is forced to roll harmonically around the center of the bottom wall. The roll motion of the tank is governed by

$$\theta = \alpha \theta_0 \sin\left(\frac{2\pi}{T} t\right) \quad (23)$$

where  $\theta_0$  is the amplitude of the roll motion and selected as  $4^\circ$ ,  $T$  is the rotation period and set as 1.6312 s ( $0.85T_N$ ). In the initial stage, the roll motion is buffered by the coefficient  $\alpha$  in Eq. (23), which is defined as

$$\alpha = \begin{cases} 0.5 \left[ 1 + \tanh\left(\frac{2\pi}{T} t - \pi\right) \right] & t < T \\ 1.0 & t \geq T \end{cases} \quad (24)$$

In present simulations, the model is dispersed by particles with an initial spacing size ( $l_0$ ) of 0.002 m and the total number of particles is 25,567. For the fluid analysis, time step size is set as 0.0002 s which satisfy the Courant–Friedrichs–Lewy (CFL) condition.

$$\Delta t_f \leq \frac{Cl_0}{V_{\max}} \quad (25)$$

where the upper bound of Courant number  $C$  is considered as 0.2 according to (Koshizuka and Oka, 1996),  $V_{\max}$  is the maximum velocity of particle. Detailed parameters for fluid and structural analysis are presented in Table 2. To investigate the influence of inherent material properties of the elastic tank on the sloshing flow and structural response, elasticity of both lateral tank walls with different stiffness by varying the Young's modulus ( $E$ ) is taken into account and corresponding cases are shown in Table 3. For the structural analysis, Rayleigh's damping has been added to the structure with a factor of  $\alpha_1 = 0.0128$  for the mass-proportional contribution to the damping and  $\alpha_2 = 5.01e^{-7}$  for the

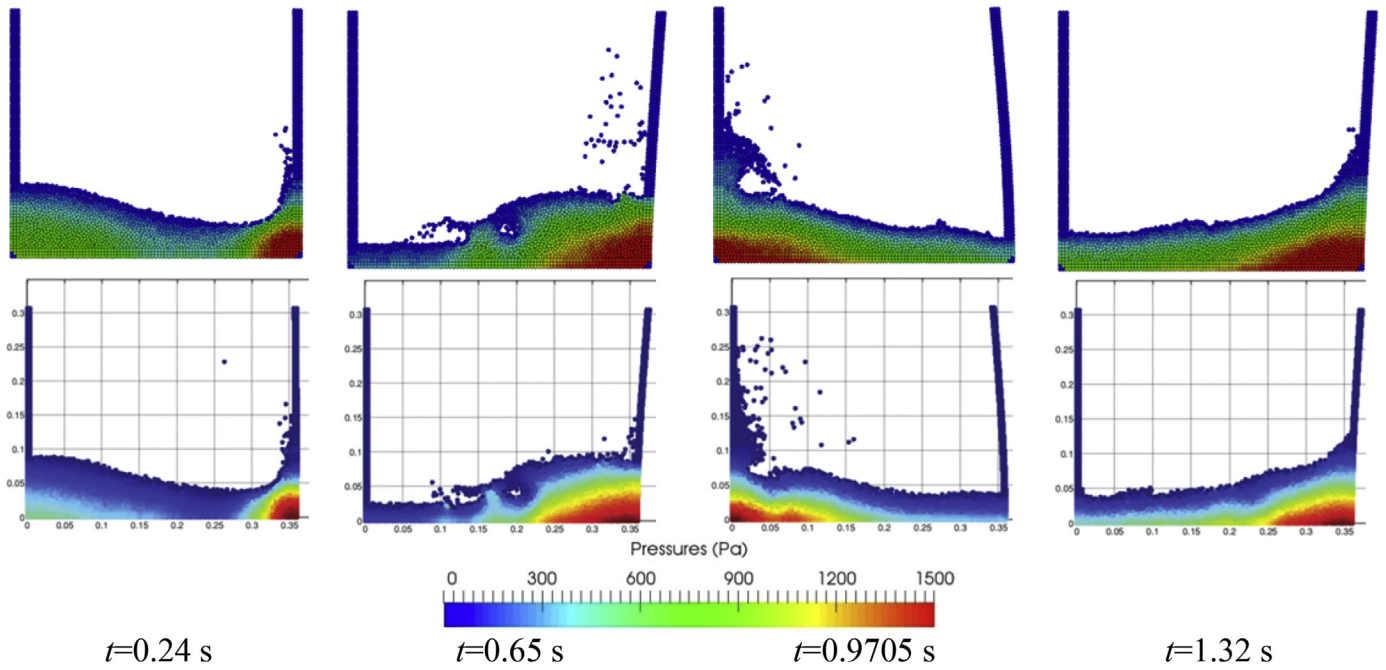


Fig. 6. Comparison of pressure contours, free surface profiles and deformations of the elastic wall (Up: present result; Down: numerical result from Sun et al., 2015).

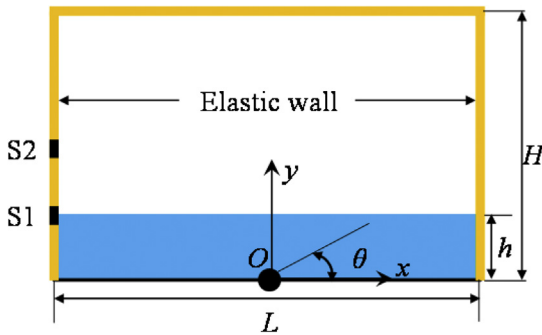


Fig. 7. Schematic sketch of liquid sloshing in a forced rolling tank.

Table 2  
Parameters for fluid and structural analysis.

Parameters	Values	Parameters	Values
Fluid density (kg/m <sup>3</sup> )	998	Structure density (kg/m <sup>3</sup> )	1800
Kinematic viscosity (m <sup>2</sup> /s)	1 × 10 <sup>-6</sup>	Thickness of tank wall (m)	0.002
Gravitational acceleration (m/s <sup>2</sup> )	9.81	Elements per lateral wall	254
Particle spacing (m)	0.002	Damping coefficients α <sub>1</sub>	0.0128
Total number of particles	25,351	Damping coefficients α <sub>2</sub>	5.01 × 10 <sup>-7</sup>
Fluid time step size (s)	2 × 10 <sup>-4</sup>	Structural time step size (s)	2 × 10 <sup>-4</sup>

Table 3  
Simulation cases.

Cases	A	B	C	D	E	F	G	H	I
Young's modulus (GPa)		80	70	60	50	40	30	20	10

stiffness-proportional contribution. In addition, the sloshing in a rigid tank (Case A in Table 3) is also simulated to show the difference in

comparison with results regarding elastic tank, and the stiffness of rigid tank is assumed for an infinitely large value.

#### 4.2. Simulation results

##### 4.2.1. Free surface evolutions

Fig. 8 shows the deformations of tank walls and evolutions of free surface corresponding to the effects of structural elasticity. The sloshing behaviors are qualitative compared between Case B, F, H, I with the Young's modulus varying based on the geometric proportion in the range  $E = 10\text{--}80$  GPa. In present numerical work, elasticity of both right and left lateral tank walls have been taken into account. Nevertheless, only the sloshing behaviors at near right wall of the tank are discussed here, since the similar characteristics of responses regarding the two lateral walls could be observed. As responses of tank walls are predominantly caused by the liquid impact loads, processes of the impact events are depicted by simulation snapshots from 11.08 s to 11.64 s with an interval time step 0.08 s. Generally, the whole process of impact event consists of four states, the overturning of wave crest, impacting of wave onto the lateral wall, jet and run up of the wave along the wall, drop of the liquid. Obvious differences between the four cases can be observed during these states. First, the impact event of Case B takes place at the instant  $t = 11.16$  s while it happens later for the cases with smaller Young's modulus, particularly for the Case I with an impact instant  $t = 11.24$  s. Then, for the Case B and F, up-shooting jets can be observed and run along the lateral wall up to the ceiling of tank, as shown in Fig. 8 B5–F5. Correspondingly, the maximum heights of jets which run along the distinctly deformed wall are much lower for the Case H and I, as shown in Fig. 8 H5–I5. It's mainly due to that more kinetic energy of fluid particles in horizontal direction is converted to elastic potential energy of tank wall compared with the cases with larger Young's modulus. During the state of liquid drop, fluid particles of Case H and I are intensely bounced off from the lateral wall compared with that of Case B and F, since more elastic potential energy of tank wall is converted back to the kinetic energy of fluid particles in horizontal direction.

##### 4.2.2. Displacement responses of lateral wall

Fig. 9 shows the time histories of displacements ( $d$ ) of measuring

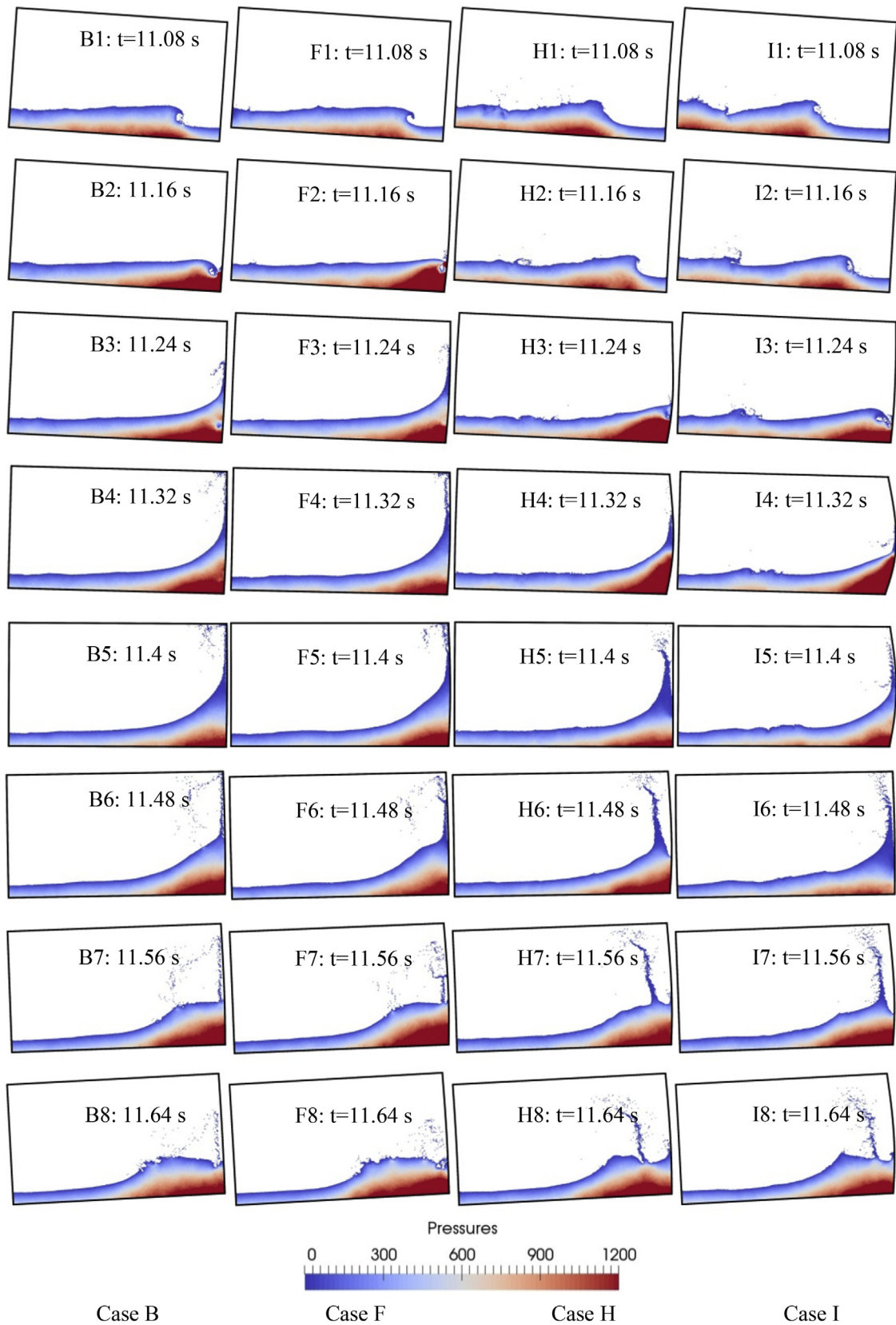


Fig. 8. Deformation of tank wall and free surface ( $E = 80/40/20/10$  GPa).

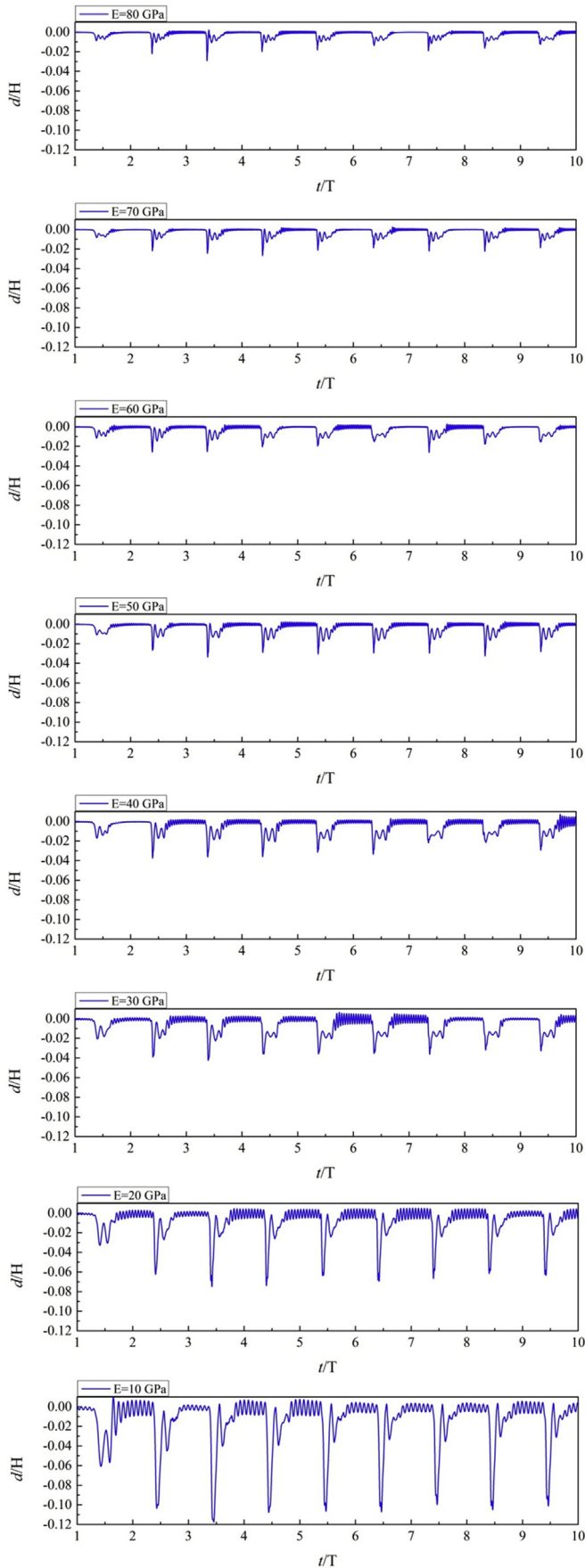


Fig. 9. Dimensionless time history of calculated displacement at measuring point S2.

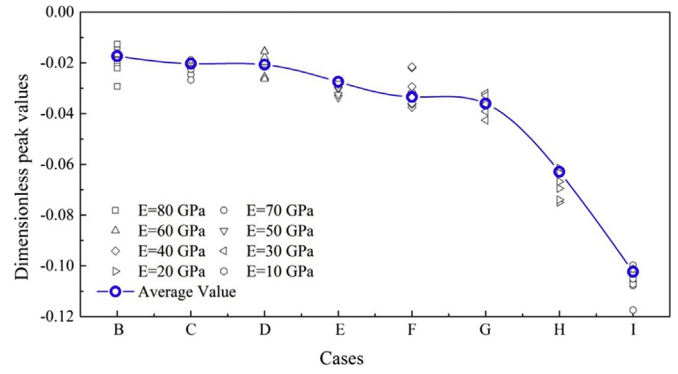


Fig. 10. Trends of dimensionless peak values of displacements.

point S2 which mounted on left wall of the elastic tank. The displacements and time have been made dimensionless with the height of lateral tank wall ( $H$ ) and excitation period ( $T$ ), respectively. It can be noticed that the tank wall oscillates with the similar characters except the amplitudes for all the cases distinguished by the Young's modulus. The large oscillation amplitudes, resulting from the peak values of impact pressure, will present with a large period approximating to the excitation period of sloshing. Besides, the oscillations with small amplitudes and small period, due to structural elastic restoring force, are also observed.

Fig. 10 shows the trends of oscillation amplitudes versus Young's modulus of the lateral wall. The large oscillation amplitudes within the dimensionless time 2–10 are presented statistically for each case. Then, the trend curve which represents the relationship between oscillation amplitude and structural stiffness are created by mean values of the statistical data. It can be noticed that the lateral wall oscillates with a larger amplitude as the reduction of structural stiffness.

Fig. 11 shows the envelope of nodal displacements of the left tank wall. Since the similar characters of the envelopes presence in all the 8 cases, only the envelope regarding to the case with the Young's modulus of 10 GPa is provided. Here, both the displacements and node positions ( $y$ ) in  $y$ -direction have been made dimensionless with the height of tank ( $H$ ). As shown in this figure, the 1st order mode shape of the lateral tank wall is prominent in the FSI event. The left wall of the tank vibrates with the much larger amplitudes in the negative  $x$ -direction, while with the

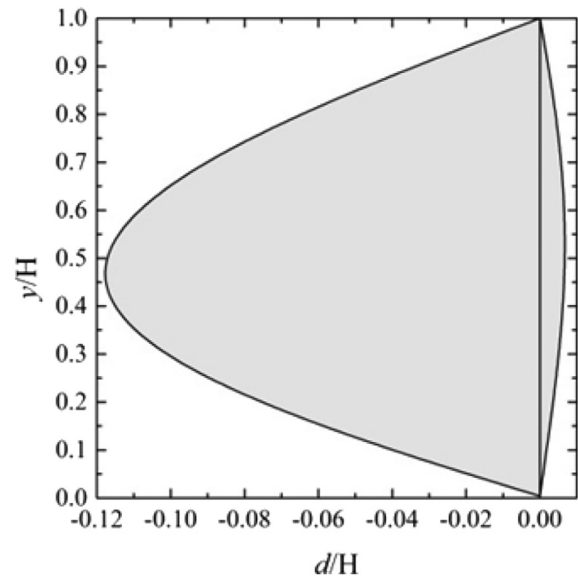


Fig. 11. Dimensionless envelopes of the displacements of lateral tank wall ( $E = 10$  GPa).

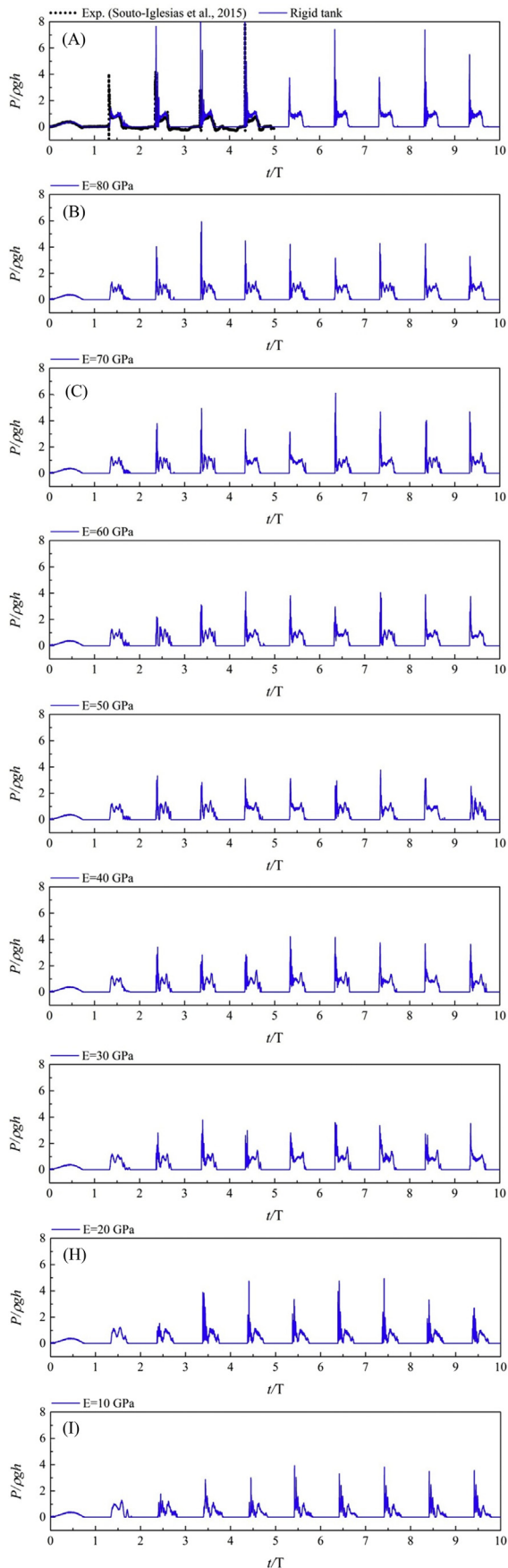


Fig. 12. Dimensionless pressure time histories at the measured point S1.

smaller amplitudes in the positive direction.

#### 4.2.3. Impact pressures on the lateral wall

As shown in Fig. 12, the pressure time histories corresponding to rigid tank and elastic tank with the Young's modulus 10–80 GPa are measured at the point S1 during the first 10 cycles. Herein, the pressure and time have been made dimensionless with the hydrostatic pressure at the reference water depth ( $h$ ) and excitation period, respectively. For the pressure in a rigid tank as shown as Fig. 12 (A), the well-known character of the impact events, “church roof shape”, is observed. Though the maximum pressure at each cycle calculated by MPS is slightly greater than the experimental data, the trend of numerical pressure variation is in agreement with the experimental result. The difference between the two results is similar to numerical result from Souto-Iglesias et al. (2015) with an explanation that a single phase simulation was conducted while the presence of air can affect the peak values and smooth the pressure curve.

For the pressures of elastic tank as shown in Fig. 12 (B–I), the maximum pressures are smaller than that in a rigid tank and patterns of impact pressures are different in comparison with the classic “church roof shape”. Details of the differences can be revealed by the closer view of the pressure time signals in Fig. 13. The shapes of the pressure time histories immediately after the peaks regarding the elastic tanks present much larger amplitude oscillations, particularly for the tanks with smaller stiffness. It can be explained that the violent transverse motions of fluid particles are incited by the vibrations of lateral tank walls, as noticeable in Fig. 8.

In Fig. 14, the dimensionless duration time ( $\Delta t$ ) and start instant ( $t_{\text{impact}}$ ) of impact events are plotted versus structural stiffness. The duration time of impact event is illustrated in previous Fig. 13 and can be defined by the difference between the end ( $t_{\text{end}}$ ) and start instants in each impact cycle. An interesting phenomenon can be noticed in Fig. 14 that the duration time of impact events increase as the decrease of structural stiffness. Besides, the start instants of impact events in elastic tanks lag in comparison with that of rigid tank. It can be observed from the evolutions of free surface in previous Fig. 8.

#### 4.2.4. Discussion of frequency responses

During the analysis of variations of pressure and structural response in frequency domain, two essential frequencies should be kept in mind, including the 1st order dry frequency of lateral tank wall  $f_{Nd}$  and the wetted frequency  $f_{Nw}$ . In this study, the dry frequency  $f_{Nd}$  and the wetted frequency  $f_{Nw}$  can be obtained by the software MSC Nastran.

According to the previous mentioned time histories of structural displacements in Fig. 9, the tank wall vibrates with large oscillation amplitudes during the impact event and with small amplitudes during the sloshing wave progressing to the other side of the tank. In the study of Lugni et al. (2014), the behavior of the wall within one sloshing period can be characterized as the quasi-static regime, the hydroelastic regime and the free-vibration regime, as the notation regime 1, regime 2 and regime 3 demonstrated in the Fig. 15. During the quasi-static stage, the elastic wall deforms as the front of sloshing wave approaches and impacts onto it. The duration of this stage can be recorded as  $\Delta t$ , and the inverse of this characteristic time scale ( $f_s$ ) is added in Table 4. By transforming the signals of the structural displacement histories corresponding to the last two regimes using the Fourier method, two response frequencies  $f_h$  and  $f_f$  can be obtained. Here,  $f_h$  and  $f_f$  represent the frequencies regarding the hydroelastic regime and the free-vibration regime, respectively. For all the cases with different Young's modulus, the typical response frequencies are summarized in Table 4. The error of the frequency of free-vibration regime  $f_f$  relative to the dry frequency  $f_{Nd}$  is represented by  $Err$  ( $Err = (f_f - f_{Nd})/f_{Nd}$ ). It can be noticed that the two frequencies are in good agreement. By contrast, the frequencies  $f_h$  are much smaller than the dry frequency  $f_{Nd}$  for all the eight cases.

According to the experimental study of hydroelastic slamming response of an elastic tank by Lugni et al. (2014), the response frequency

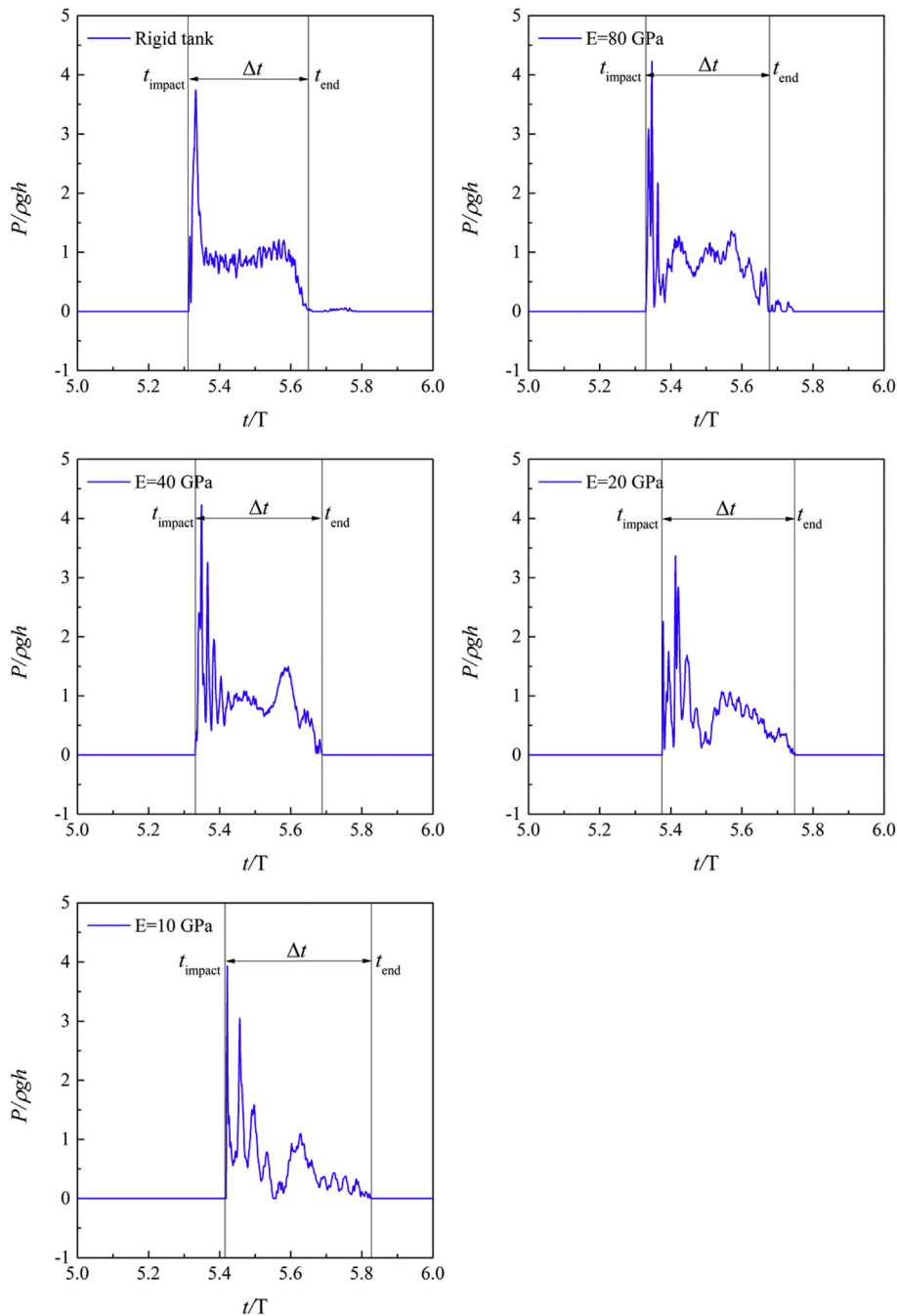


Fig. 13. Zoom of Fig. 12 over the sixth impact event.

$f_h$  may be effected by the added mass of water acting on the tank wall. To confirm the conjecture, the wetted frequencies regarding varying water heights on the lateral wall are calculated based on the software MSC Nastran, as shown in Fig. 16. For all the cases with different Young's modulus, the wetted natural frequencies  $f_{Nw}$  decrease as the rising of the water on the lateral wall. The equivalent heights  $h_w$  regarding the frequencies  $f_h$  are in the range 0.2–0.3 m, which are the dominant wetted heights on the tank wall during the impact events, and can be observed from the Fig. 8.

## 5. Conclusions

In this paper, a fully Lagrangian FSI solver is primarily implemented

based on the MPS-FEM coupled method. Feasibility of the present solver for FSI problems with free surface is validated by the benchmark test of dam-break flow impacting onto an elastic tank wall, and good agreements between the present numerical results and the published data are achieved.

Then, the interaction between the violent sloshing flow and a liquid tank with elastic lateral walls is simulated. By varying the Young's modulus, the influences of the structural elasticity on the sloshing phenomenon are investigated. According to the evolutions of free surfaces, it can be observed that the impact events of the sloshing in a tank with small Young's modulus happen later than those in a more rigid tank, and the phenomenon of fluid particles bouncing off from the tank's lateral walls is obvious. According to the pressure histories measured on the lateral walls, fluctuations of the pressure signals, which are induced by

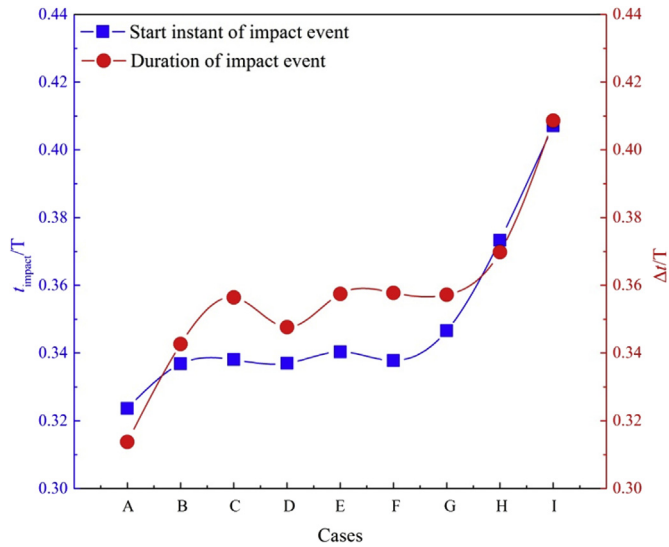


Fig. 14. Start and duration of the impact event.

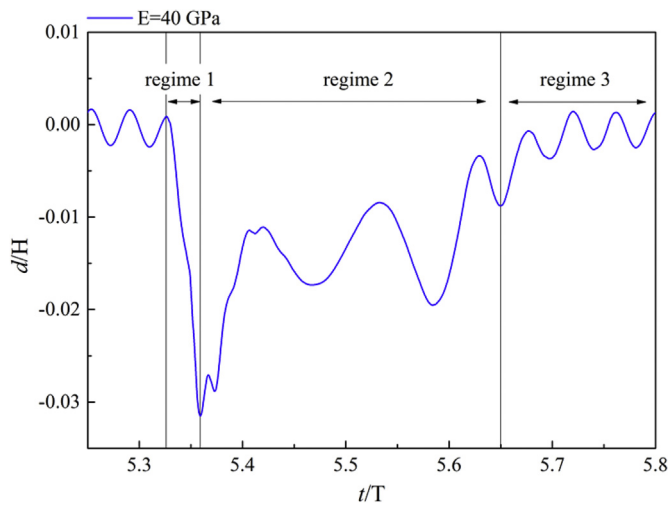


Fig. 15. Demonstration of the displacement response regimes ( $E = 40$  GPa).

Table 4  
Comparisons of response frequencies.

Cases	$E$ (GPa)	$f_{Nd}$ (Hz)	$f_s$ (Hz)	$f_h$ (Hz)	$f_f$ (Hz)	Err (%)
Case B	80	24.22	21.28	9.32	23.36	-3.6
Case C	70	22.65	19.52	8.45	20.93	-7.6
Case D	60	20.97	18.75	7.5	20.19	-3.7
Case E	50	19.15	22.25	7.34	18.02	-5.9
Case F	40	17.1	19.3	6.31	16.3	-4.7
Case G	30	14.83	19.12	5.3	13.97	-5.8
Case H	20	12.11	18.18	3.62	11.24	-7.2
Case I	10	8.56	16.13	3.23	7.96	-7.1

the vibrations of the elastic walls, are observed. Besides, the structural responses are also presented. The response frequencies  $f_f$  regarding the free-vibration regime are in agreement with the dry natural frequencies  $f_{Nd}$ . By contrast, the wetted frequencies  $f_h$  are much smaller than the dry frequency  $f_{Nd}$  for all the eight cases since the effects of the added mass of water acting on the tank wall.

In sum, as a preliminary study, the MPS-FEM coupled is a good choice for the investigation of sloshing involving fluid structure interaction. However, there are still some key issues of this FSI problem to be solved. For instance, the cavity will be entrapped during the sloshing wave

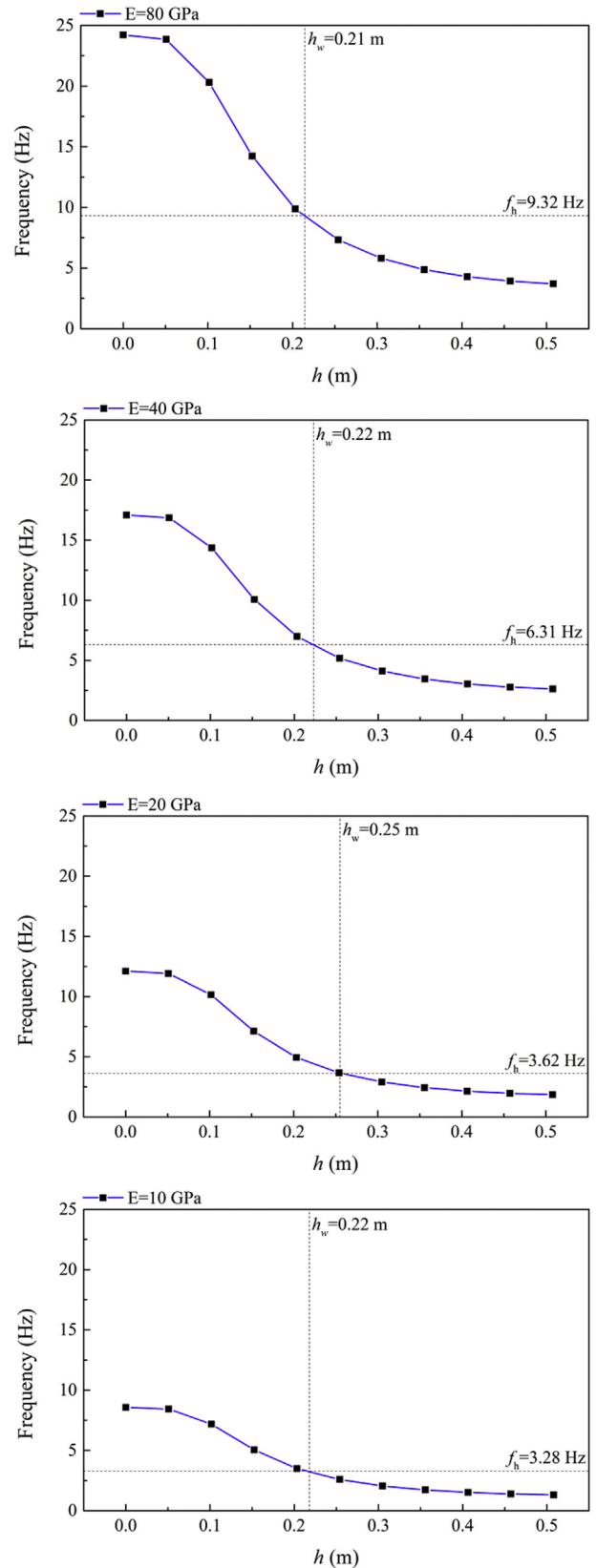


Fig. 16. Wetted frequencies regarding varying water heights on the lateral wall ( $E = 80/40/20/10$  GPa).

impacting onto the lateral wall, and may effects the characterization of the hydrodynamic loads. To obtain the more accurate impact pressures, the presented FSI solver is planned to be improved with the two-phase

model.

## Acknowledgement

This work is supported by the National Natural Science Foundation of China (51490675, 51379125, 11432009, 51579145), Chang Jiang Scholars Program (T2014099), Shanghai Excellent Academic Leaders Program (17XD1402300), Program for Professor of Special Appointment (Eastern Scholar) at Shanghai Institutions of Higher Learning (2013022), Innovative Special Project of Numerical Tank of Ministry of Industry and Information Technology of China (2016-23/09) and Lloyd's Register Foundation for doctoral student, to which the authors are most grateful.

## References

- Faltinsen, O.M., Timokha, A.N., 2009. *Sloshing*. Cambridge University Press, New York.
- Fossa, M., Rizzo, C.M., Tani, G., Viviani, M., 2012. Simulations of a sloshing experiment by FEM CFD and FEM FSI approaches. In: *Proceedings of the Twenty-second International Offshore and Polar Engineering Conference (ISOPE2012)*, pp. 530–537. Rhodes, Greece.
- Graczyk, M., Moan, T., Wu, M.K., 2007. Extreme sloshing and whipping-induced pressures and structural response in membrane LNG tanks. *Ships Offshore Struct.* 2 (3), 201–216.
- Hsiao, K.M., Lin, J.Y., Lin, W.Y., 1999. A consistent co-rotational finite element formulation for geometrically nonlinear dynamic analysis of 3-D beams. *Comput. Methods Appl. Mech. Eng.* 169, 1–18.
- Hwang, S.C., Khayyer, A., Gotoh, H., Park, J.C., 2014. Development of a fully Lagrangian MPS-based coupled method for simulation of fluid-structure interaction problems. *J. Fluids Struct.* 50, 497–511.
- Hwang, S.C., Park, J.C., Gotoh, H., Khayyer, A., Kang, K.J., 2016. Numerical simulations of sloshing flows with elastic baffles by using a particle-based fluid-structure interaction analysis method. *Ocean. Eng.* 118, 227–241.
- Idelsohn, S.R., Marti, J., Limache, A., Onate, E., 2008. Unified Lagrangian formulation for elastic solids and incompressible fluids: application to fluid-structure interaction problems via the PFEM. *Comput. Methods Appl. Mech. Eng.* 197, 1762–1776.
- Ito, H., Suh, Y., Chun, S., 2008. A direct assessment approach for structural strength evaluation of cargo containment system under sloshing inside LNGC tanks based on fluid structure interaction. In: *Proceedings of the 27th International Conference on Offshore Mechanics and Arctic Engineering (OMAE2008)*, pp. 835–845. Estoril, Portugal.
- Jia, D., Agrawal, M., Wang, C., Shen, J., Malachowski, J., 2015. Fluid-structure interaction of liquid sloshing induced by vessel motion in floating LNG tank. In: *Proceedings of the 34th International Conference on Offshore Mechanics and Arctic Engineering (OMAE2015)*. Newfoundland, Canada, OMAE2015–41463.
- Kim, Y., 2015. Rapid response calculation of LNG cargo containment system under sloshing load using wavelet transformation. *Int. J. Nav. Archit. Ocean Eng.* 5 (2), 227–245.
- Koshizuka, S., Oka, Y., 1996. Moving particle semi-implicit method for fragmentation of incompressible fluid. *Nucl. Sci. Eng.* 123, 421–434.
- Koshizuka, S., Nobe, A., Oka, Y., 1998. Numerical analysis of breaking waves using the Moving Particle Semi-implicit method. *Int. J. Numer. Methods Fluids* 26 (7), 751–769.
- Lee, B.H., Park, J.C., Kim, M.H., Hwang, S.C., 2011. Step-by-step improvement of MPS method in simulating violent free-surface motions and impact-loads. *Comput. Methods Appl. Mech. Eng.* 200, 1113–1125.
- Lee, C.S., Cho, J.R., Kim, W.S., Noh, B.J., Kim, M.H., Lee, J.M., 2015. Evaluation of sloshing resistance performance for LNG carrier insulation system based on fluid-structure interaction analysis. *Int. J. Nav. Archit. Ocean Eng.* 5 (1), 1–20.
- Liao, K.P., Hu, C.H., 2013. A coupled FDM-FEM method for free surface flow interaction with thin elastic plate. *J. Mar. Sci. Technol.* 18, 1–11.
- Liu, D., Lin, P., 2009. Three-dimensional liquid sloshing in a tank with baffles. *Ocean. Eng.* 36 (2), 202–212.
- Lugni, C., Bardazzi, A., Faltinsen, O.M., Graziani, G., 2014. Hydroelastic slamming response in the evolution of a flip-through event during shallow-liquid sloshing. *Phys. Fluids* 26 (3). <https://doi.org/10.1063/1.4868878>, 102107–104.
- Mitra, S., Wang, C.Z., Reddy, J.N., Khoo, B.C., 2012. A 3-D fully coupled analysis of nonlinear sloshing and ship motion. *Ocean. Eng.* 39 (1), 1–13.
- Mitsume, N., Yoshimura, S., Murotani, K., Yamada, T., 2014. MPS-FEM partitioned coupling approach for fluid-structure interaction with free surface flow. *Int. J. Comput. Methods* 11 (4), 4157–4160.
- Newmark, N.M., 1959. A method of computation for structural dynamics. *J. Eng. Mech. Div.* 85 (3), 67–94.
- Paik, K.J., Carrica, P.M., 2014. Fluid-structure interaction for an elastic structure interacting with free surface in a rolling tank. *Ocean. Eng.* 84, 201–212.
- Souto-Iglesias, A., Bulian, G., Botia-Vera, E., 2015. A set of canonical problems in sloshing. Part 2: influence of tank width on impact pressure statistics in regular forced angular motion. *Ocean. Eng.* 105, 136–159.
- Sun, Z., Djidjeli, K., Xing, J.T., Cheng, F., 2015. Modified MPS method for the 2D Fluid structure interaction problem with free surface. *Comput. Fluids* 122, 47–65.
- Tang, Z.Y., Wan, D.C., 2015. Numerical simulation of impinging jet flows by modified MPS method. *Eng. Comput.* 32 (4), 1153–1171.
- Tang, Z.Y., Zhang, Y.L., Wan, D.C., 2016a. Multi-resolution MPS method for free surface flows. *Int. J. Comput. Methods* 13 (4), 1641018.
- Tang, Z.Y., Zhang, Y.L., Wan, D.C., 2016b. Numerical simulation of 3D free surface flows by overlapping MPS. *J. Hydrodyn.* 28 (2), 306–312.
- Wang, B., Kim, J.W., 2007. Strength evaluation of LNG containment system considering fluid-structure interaction under sloshing impact pressure. In: *Proceedings of the 26th International Conference on Offshore Mechanics and Arctic Engineering (OMAE2007)*, pp. 545–552. San Diego, California, USA.
- Zhang, Y.L., Wan, D.C., 2017. Numerical study of interactions between waves and free rolling body by IMPS method. *Comput. Fluids* 155, 124–133.
- Zhang, Y.X., Wan, D.C., Hino, T., 2014. Comparative study of MPS method and level-set method for sloshing flows. *J. Hydrodyn.* 26 (4), 577–585.
- Zhang, Y.L., Tang, Z.Y., Wan, D.C., 2016. Numerical investigations of waves interacting with free rolling body by modified MPS method. *Int. J. Comput. Methods* 13 (4), 1641013.
- Zhao, W., Yang, J., Hu, Z., Tao, L., 2014. Coupled analysis of nonlinear sloshing and ship motions. *Appl. Ocean Res.* 47 (47), 85–97.